Supporting Information

Coordination-based pH-Responsive Metal-Nucleotide System: pH-Responsive Fluorescence Switch and SHG Crystalline Material

Pei Zhou, Chong Wang, Qi-ming Qiu, Jian-feng Yao, Chuan-Fang Sheng, and Hui Li*

Key Laboratory of Clusters Science of Ministry of Education, School of Chemistry, Beijing Institute of Technology, Beijing, 100081, P. R. China.

*E-mail address: lihui@bit.edu.cn

Tel: 86-10-68912667

Contents

Section 1 Acidity Constants for 5'-Nucleoside Monophosphates.

Table S1. Acidity Constants for 5'-Nucleoside Monophosphates. (pKa. near 25 ℃ and 0.1 M ionic strength)

5'-NMP	N1	N7	N9	N3
AMP	~1.1 or 0.2±0.5	3.8		
GMP	9.5	2.4		
IMP	8.9	1.3		
CMP			-	4.4
UMP			-	9.6
TMP			-	9.9

Section 2. UV-vis and Fluorescence Titration Spectra

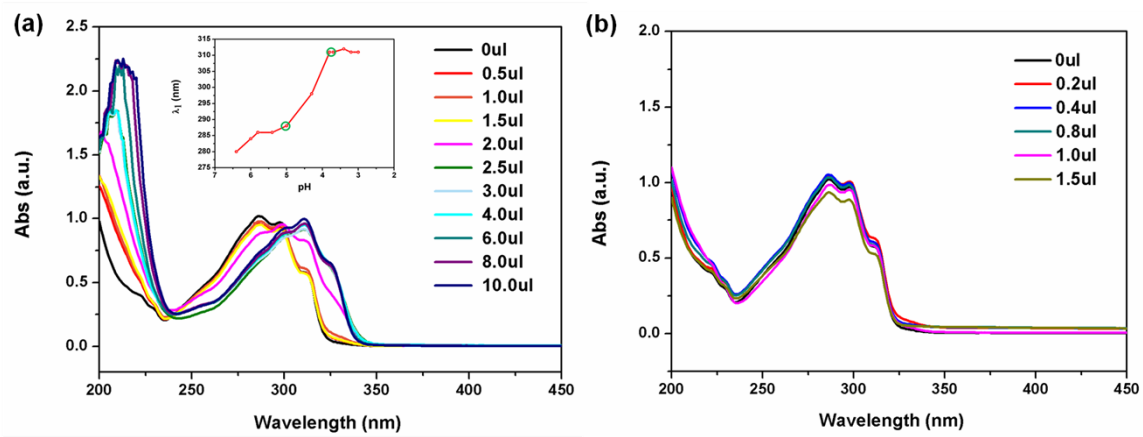

Figure S1. UV-visible absorption spectra recorded during titration of a solution of CMP-bpe-Mn(II) ([CMP]=[bpe]=[Mn^{2+}]=5×10^{-5}mol/L^{-1}) with HNO_3 (0.8M, *a*) or NaOH(1M, *b*). (*insert*) The changes of λ_1 (wavelength of the highest energy absorption peak) at different pH value for the solution of complex **1** by addition of HNO_3. λ_1 shows obvious red shift and a new absorption peak near 325nm appears at pH<5, stating that there is a new species.

Table S2. The relationship between pH value and the acid/alkali addition in the solution of (a) bpe-Mn and (b) bpe-CMP ([bpe-Mn]=[bpe-CMP]=5×10^{-5}mol/L).

(a)

$V_{(H+,\mu l)}$	10.0	8.0	6.0	4.0	3.0	2.5	2.0	1.5	1.0	0.5	0					
$V_{(OH-,\mu l)}$											0	0.2	0.4	0.8	1.0	1.5
$pH_{(1)}$	3.22	3.38	3.91	4.12	4.82	5.09	5.53	6.03	6.41	6.79	7.11	.7.72	8.11	8.18	8.32	8.54
$pH_{(2)}$	3.22	3.37	3.58	3.80	4.25	5.28	5.96	6.40	6.63	7.04	7.25	7.52	7.98	8.09	8.21	8.44
$pH_{(3)}$	3.21	3.38	3.60	4.09	4.36	5.32	5.78	6.32	6.66	6.96	7.23	7.49	8.02	8.13	8.20	8.49
$pH_{(eve)}$	3.21	3.38	3.40	4.00	4.47	5.23	5.75	6.25	6.57	6.93	7.20	7.58	8.03	8.13	8.24	8.48

(b)

$V_{(H+,\mu l)}$	10.0	8.0	6.0	4.0	3.0	2.5	2.0	1.5	1.0	0.5	0					
$V_{(OH-,\mu l)}$											0	0.2	0.4	0.8	1.0	1.5
$pH_{(1)}$	2.92	3.02	3.22	3.25	4.19	4.49	5.11	5.95	6.34	6.67	6.98	.7.31	7.38	7.49	7.78	8.40
$pH_{(2)}$	2.92	3.02	3.25	3.27	4.13	4.62	4.98	5.57	5.94	6.23	6.38	7.08	7.19	7.55	7.84	8.43
$pH_{(3)}$	2.93	3.00	3.29	3.32	4.43	4.67	5.05	5.76	6.04	6.40	6.62	7.10	7.35	7.44	7.80	8.41
$pH_{(eve)}$	2.92	3.01	3.25	3.28	4.22	4.66	5.05	5.76	6.10	6.43	6.66	7.16	7.30	7.49	7.81	8.41

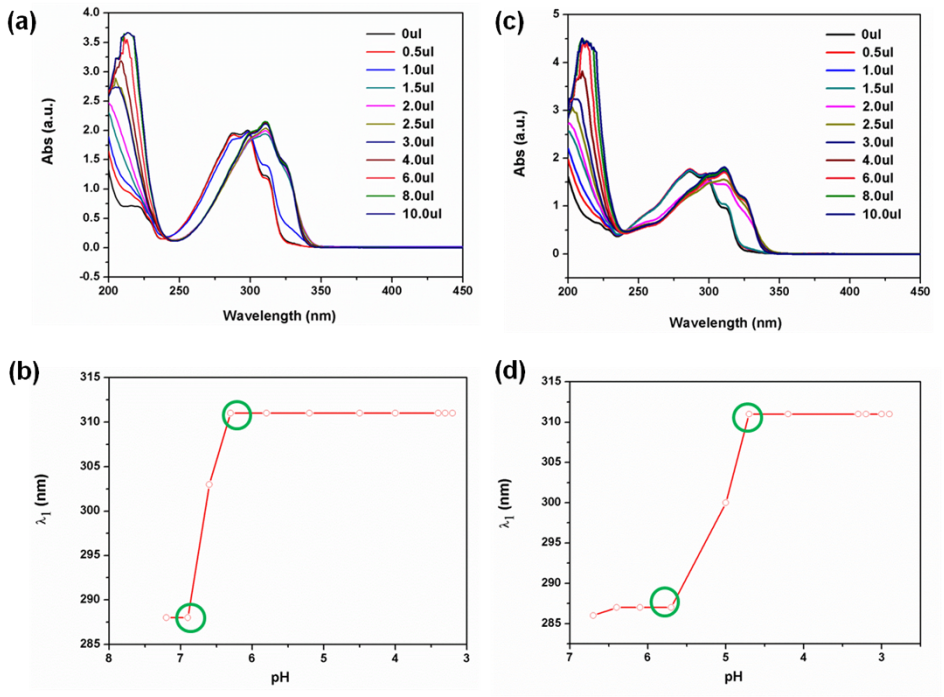

Figure **S2**. UV-visible absorption spectra recorded during titration of a solution of (a) bpe-Mn and (c) bpe-CMP with 0.8M HNO_3. [bpe-Mn] = [bpe-CMP]=5×10^{-5}mol/L^{-1}). The changes of λ_1 at different pH value for (b) bpe-Mn and (d) bpe-CMP, which also show red shift as pH reduce.

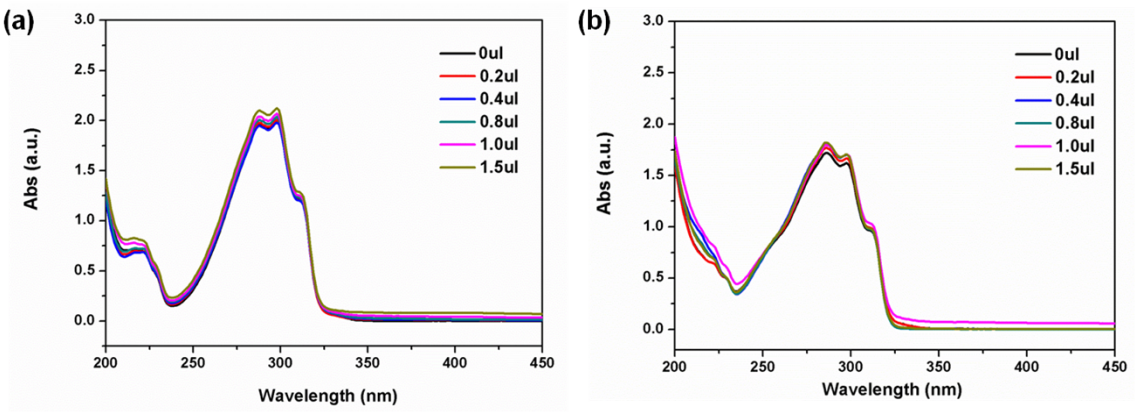

Figure S3. UV-visible absorption spectra recorded during titration of a solution of (a) bpe-Mn and (b) bpe-CMP with1.0M NaOH. [bpe-Mn] = [bpe-CMP] = 5×10^{-5}mol/L^{-1}).

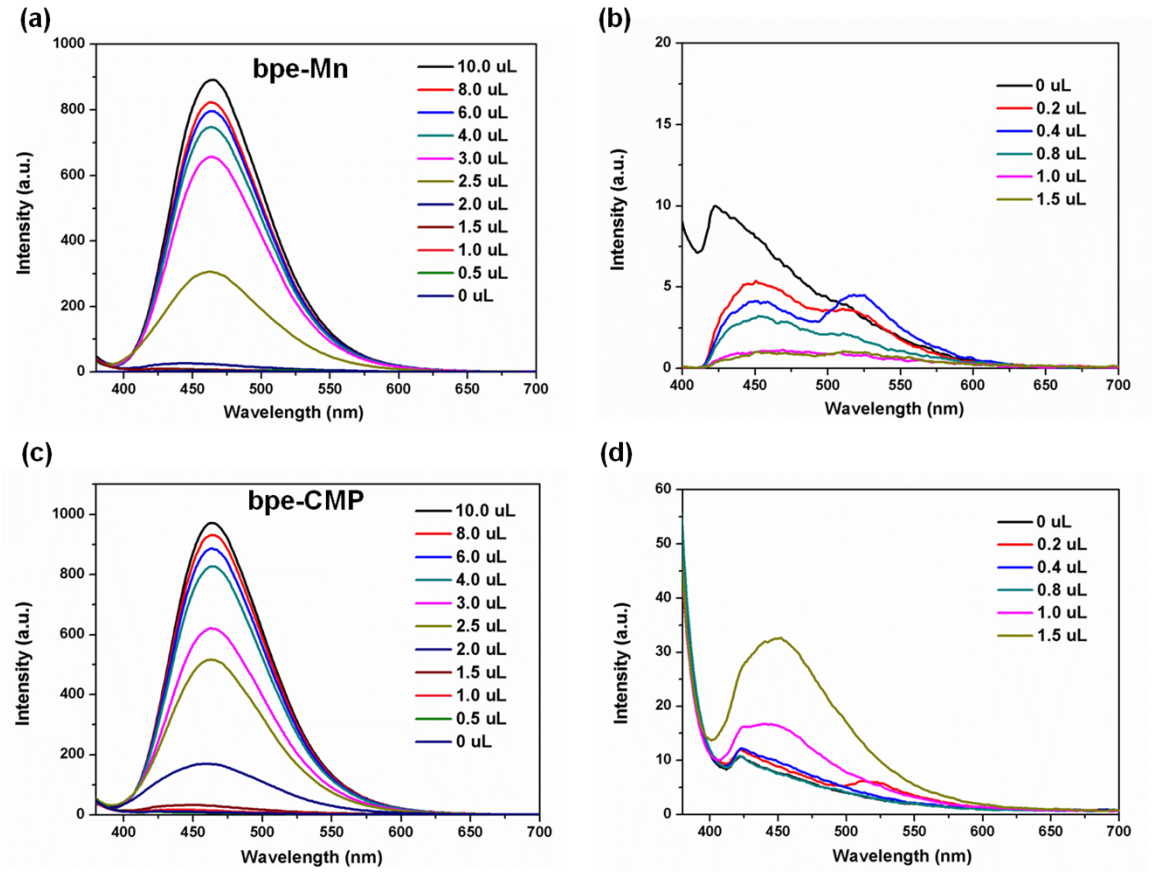

Figure S4. Fluorescence titration spectra (λ_{ex}=365nm) of a solution of bpe-Mn and bpe-CMP ([bpe-Mn] = [bpe-CMP] = 5.0×10^{-5} molL^{-1}) with HNO_3 (0.8M, *a and c*) or NaOH(1M, *b and d*).

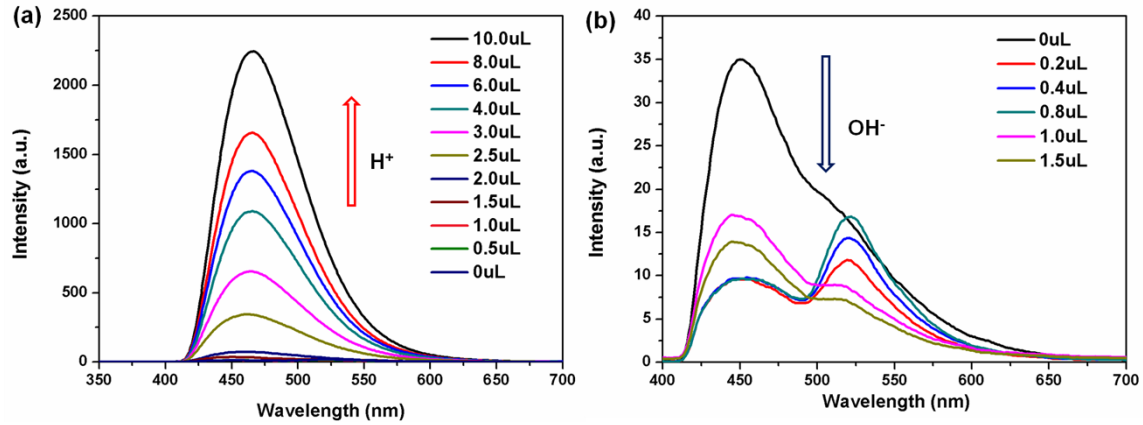

Figure S5. Fluorescence titration spectra (λ_{ex}=365nm) of a solution of CMP-bpe-Co ([bpe]=[CMP]=[Co^{2+}]= 5.0×10^{-5} molL^{-1}) with HNO_3 (0.8M, *a and c*) or NaOH(1M, *b and d*).

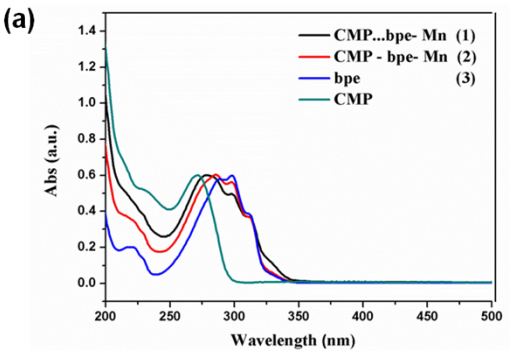

(b)

Abs. Peak(nm)	λ_1	λ_2	λ_3
bpe	289	300	313
CMP	273	--	--
1	280	300	313
2	287	300	313

Figure S6. Room–temperature UV-vis absorption spectra (a) and the relative absorption peaks (b) in water solution of complex **1** (black line), **2** (red line), bpe (blue line) and CMP (cyan line). [**1**] = [**2**] = [bpe] = [CMP] = 5.0×10^{-5} $molL^{-1}$. Samples are dissolved in aqueous solution and the thickness of sample cell is 1cm.

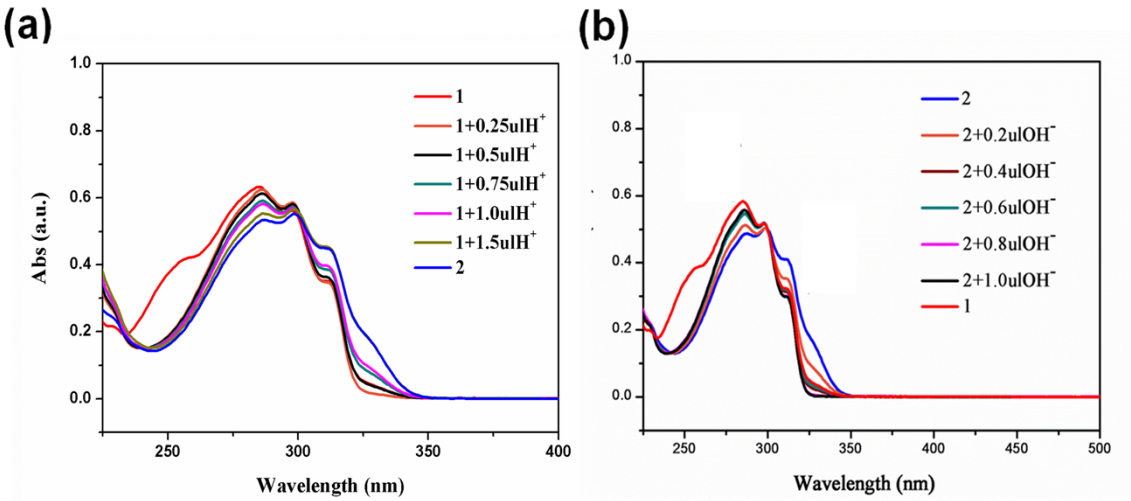

Figure S7. UV-vis titration spectra for the reversible convert between **1** and **2** adjusted by 1M HCl or NaOH.

Section 3 Crystallography date and Structural Information.

Table S3. Crystal Data and Structure Refinement of Complexes

Complex	**1**	**2**	**3**	**5**
Empirical formula	$C_{21}H_{36}N_5O_{15}PMn$	$C_{60}H_{94}N_{16}O_{43}P_4Mn_2$	$C_{60}H_{64}Cl_2MnN_{10}O_{15}$	$C_{60}H_{94}N_{16}O_{43}P_4Co_2$
Formula weight	684.46	1961.27	1291.5	1969.25
Wavelength (Å)	0.71073	0.71073	0.71073	0.71073
Temperature(K)	153.15(2)	296(2)	293(2)	153.15(2)
Crystal system	Monoclinic	Orthorhombic	Monoclinic	Orthorhombic

space group	$P2_1$	$P2_12_12_1$	$P2_1/c$	$P2_12_12_1$
a (Å)	9.2640(19)	13.870(3)	16.568(3)	13.666(3)
b (Å)	12.020(2)	14.057(3)	13.671(3)	13.939(3)
c (Å)	13.833(3)	20.780(5)	29.949(10)	20.703(4)
α (º)	90	90	90	90
β (º)	106.95(3)	90	111.38(3)	90
γ (º)	90	90	90	90
Volume ($Å^3$)	1473.5(5)	4051.5(16)	6317(3)	3943.7(14)
Z	2	2	4	2
$D_{calc.}$ (g/cm^{-3})	1.543	1.608	1.358	1.658
Abs coeff (mm^{-1})	0.581	0.501	0.367	0.615
F (000)	714	2040	2692	2048
θ Range /°	2.36-29.14	1.75-28.28	3.03-27.49	1.97-29.14
Reflections collected / unique	13197/7588	24639 / 9673	50160/14436	34938/10554
Completeness to theta	29.14, 99.4 %	28.28, 98.3 %	27.49, 99.7%	29.14, 99.8%
GOF on F^2	0.967	1.044	1.164	1.042
R1,wR2 [I >2σ(I)]	0.0394, 0.0686	0.0609, 0.1432	0.0959, 0.2410	0.0645, 0.11679
R1,wR2 (all data)	0.0497, 0.0725	0.0977, 0.1627	0.1164, 0.2565	0.0781, 0.1803
Flack parameter	-0.001(12)	-0.03(3)	--	-0.009(17)

Table S4. Selected Bond Lengths (Å) and Angles (deg) in Coordination Metal Environments in **1 , 2 and 3**[a].

1			
Mn(1)-O(9)	2.1252(17)	Mn(1)-O(8)	2.1372(17)
Mn(1)-O(11)	2.2011(17)	Mn(1)-O(10)	2.2133(17)
Mn(1)-N(3)	2.2578(19)	Mn(1)-N(4)	2.2699(19)
O(9)-Mn(1)-O(8)	91.53(7)	O(9)-Mn(1)-O(11)	173.83(7)
O(8)-Mn(1)-O(11)	92.42(7)	O(9)-Mn(1)-O(10)	90.11(7)
O(8)-Mn(1)-O(10)	177.87(7)	O(11)-Mn(1)-O(10)	86.06(7)

O(9)-Mn(1)-N(3)	92.23(7)	O(8)-Mn(1)-N(3)	88.26(7)
O(11)-Mn(1)-N(3)	92.62(7)	O(10)-Mn(1)-N(3)	90.32(7)
O(9)-Mn(1)-N(4)	89.52(7)	O(8)-Mn(1)-N(4)	92.11(7)
O(11)-Mn(1)-N(4)	85.61(7)	O(10)-Mn(1)-N(4)	89.26(7)
N(3)-Mn(1)-N(4)	178.20(8)		

2

Mn(1)-O(6)	2.146(3)	Mn(1)-O(3)	2.154(3)
Mn(1)-O(5)	2.198(3)	Mn(1)-N(8)	2.264(4)
Mn(1)-O(4)	2.284(4)	Mn(1)-N(7)	2.264(4)
O(6)-Mn(1)-O(3)	92.72(13)	O(6)-Mn(1)-O(5)	86.79(11)
O(3)-Mn(1)-O(5)	177.82(12)	O(6)-Mn(1)-N(8)	95.98(15)
O(3)-Mn(1)-N(8)	90.39(14)	O(5)-Mn(1)-N(8)	91.78(14)
O(6)-Mn(1)-O(4)	178.62(12)	O(3)-Mn(1)-O(4)	88.66(13)
O(5)-Mn(1)-O(4)	91.83(13)	N(8)-Mn(1)-O(4)	83.97(15)
O(6)-Mn(1)-N(7)	92.58(14)	O(3)-Mn(1)-N(7)	86.14(13)
O(5)-Mn(1)-N(7)	91.75(13)	N(8)-Mn(1)-N(7)	170.83(14)
O(4)-Mn(1)-N(7)	87.55(15)		

3

Mn(1)-O(19)	2.060(3)	Mn(1)-O(8)	2.062(3)
Mn(1)-N(4)	2.115(3)	Mn(1)-N(2)	2.112(3)
Mn(1)-N(1)	2.136(3)	Mn(1)-N(3)	2.152(3)
O(19)-Mn(1)-O(8)	178.51(11)	O(19)-Mn(1)-N(4)	90.28(11)
O(8)-Mn(1)-N(4)	91.13(11)	O(19)-Mn(1)-N(2)	87.79(11)
O(8)-Mn(1)-N(2)	91.79 (11)	O(19)-Mn(1)-N(1)	91.18(12)
O(8)-Mn(1)-N(1)	89.30(11)	N(4)-Mn(1)-N(1)	89.48(12)
N(2)-Mn(1)-N(1)	177.59(12)	O(19)-Mn(1)-N(3)	89.50(10)
O(8)-Mn(1)-N(3)	89.08(10)	N(4)-Mn(1)-N(3)	179.54(12)
N(2)-Mn(1)-N(3)	91.24(11)	N(1)-Mn(1)-N(3)	90.93(11)
N(4)-Mn(1)-N(2)	88.34(11)		

5

Co(1)-O(2)	2.065(3)	Co(1)-O(3)	2.107(3)
Co(1)-O(4)	2.132(3)	Co(1)-N(1)	2.140(3)
Co(1)-N(2)	2.147(3)	Co(1)-O(1)	2.164(3)
O(2)-Co(1)-O(3)	91.52(11)	O(2)-Co(1)-O(4)	177.71(12)
O(3)-Co(1)-O(4)	87.04(11)	O(2)-Co(1)-N(1)	86.63(12)
O(3)-Co(1)-N(1)	91.70(12)	O(4)-Co(1)-N(1)	O(4)-Co(1)-N(1)
O(2)-Co(1)-N(2)	90.95(13)	O(3)-Co(1)-N(2)	94.24(13)
O(4)-Co(1)-N(2)	90.92(13)	N(1)-Co(1)-N(2)	173.65(14)
O(2)-Co(1)-O(1)	89.19(12)	O(3)-Co(1)-O(1)	178.59(13)
O(4)-Co(1)-O(1)	92.29(12)	N(1)-Co(1)-O(1)	89.56(13)
N(2)-Co(1)-O(1)	84.54(13)		

Table S5. Hydrogen Bond Distances (Å) and Angles (deg) in **1-3.**

D-H…A	d(D-H)	d(H…A)	d(D…A)	∠(DHA)	Symmetry transformation for acceptor
			1		
N20-H20A···O15	0.860	2.330	3.170	165.56	-x+1, y+1/2, -z+1
N20-H20B···O5	0.860	2.000	2.849	168.82	-x+1, y+1/2, -z+1
O8-H8C···O6	0.850	1.827	2.677	179.49	-x+1, y+1/2, -z+1
O8-H8D···O5	0.850	1.822	2.672	179.62	
O9-H9C···O6	0.850	1.866	2.714	175.60	
O9-H9D···O14	0.850	1.767	2.615	175.62	-x+1, y-1/2, -z+1
O10-H10C···N20	0.850	2.400	3.224	163.65	-x, y-1/2, -z+1
O10-H10D···O7	0.850	1.820	2.643	162.52	x-1, y, z
O11-H11D···O15	0.850	1.891	2.741	178.36	x-1, y, z
O11-H11C···O7	0.850	1.740	2.590	179.20	-x+1, y+1/2, -z+1
O12-H12···N1	0.820	2.032	2.852	177.74	-x+1, y-1/2, -z+2
O13-H13A···O2	0.820	1.792	2.589	163.89	-x+1, y-1/2, -z+2
O14-H14C···O11	0.850	2.069	2.918	176.04	x+1, y, z
O14-H14D···O5	0.850	1.919	2.767	176.35	
O15-H15B···O5	0.847	1.883	2.716	167.27	
O15-H15D···O12	0.850	2.080	2.887	158.36	x, y, z-1
O16-H16C··· O6	0.850	1.974	2.823	175.98	-x+1, y+1/2, -z+1
O16-H16D···O13	0.850	1.977	2.826	175.68	-x+1, y+1/2, -z+1
			2		
N3-H3A···O19	0.860	2.002	2.853	170.25	-x, y+1/2, -z+1/2
N3-H3B···O8	0.860	2.218	3.060	166.26	-x+1, y+1/2, -z+1/2
N6-H6A···O1	0.860	2.031	2.886	172.79	x, y-1/2, -z+1/2
N6-H6B···O10	0.860	2.488	3.307	159.40	-x+1, y-1/2, -z+1/2
O3-H3E···O11	0.850	1.771	2.616	172.24	-x+1, y-1/2, -z+1/2
O3-H3F···O23	0.850	1.858	2.699	170.03	-x+3/2, -y+1, z-1/2
O4-H4C···O23	0.857	2.514	3.371	179.17	-x+3/2, -y+1, z-1/2
O4-H4D···O11	0.874	1.844	2.718	178.79	
O7-H7C···O5	0.820	1.755	2.563	168.20	
O10-H10D···O22	0.820	2.107	2.712	130.52	
O14-H14A···O7	0.820	2.304	3.018	145.81	x-1/2, -y+3/2, -z
O15-H15A···O21	0.820	1.973	2.750	157.84	x, y, z-1
O16-H16···O10	0.820	1.890	2.627	148.84	x-1/2, -y+3/2, -z
O18-H18A···O8	0.820	1.829	2.637	168.19	x-1/2, -y+1/2, -z
O20-H20C···O8	0.850	2.483	3.328	172.72	x-1/2, -y+1/2, -z+1
O20-H20D···O16	0.850	2.301	3.028	143.62	x, y-1, z+1
O21-H21E···O1	0.850	2.289	3.098	159.07	x+1/2, -y+3/2, -z+1
O21-H21F···O14	0.850	2.530	3.338	159.12	x+1/2, -y+3/2, -z+1
O22-H22C···O15	0.850	2.007	2.728	142.19	x+1/2, -y+3/2, -z

O22-H22D···O23	0.850	2.229	3.041	146.04	x+1/2, -y+3/2, -z+1
O23-H23B···O18	0.850	2.156	2.687	120.28	x+1, y, z+1
O23-H23D···O20	0.850	1.978	2.828	178.41	x+1/2, -y+1/2, -z+2

3

O8-H8···N11	0.820	1.963	2.771	168.29	-x+1, -y+2, -z+1
O8-H8C···O13	0.850	1.856	2.681	163.06	x+1, y, z
O19-H19···N10	0.820	1.968	2.779	169.62	-x+2, -y+2, -z+2
O19-H19D··· O20	0.850	1.830	2.658	164.68	
O13-H13C···O21	0.849	1.909	2.754	173.61	-x, -y+1, -z+1
O13-H13D···N6	0.849	1.982	2.828	173.90	x, -y+3/2, z+1/2
O20-H20C···O22	0.850	1.910	2.759	177.44	-x+1, y+1/2, -z+3/2
O20-H20D···N5	0.851	1.898	2.749	177.67	
O21-H21C···N20	0.851	1.984	2.827	170.79	x-1, y, z
O21-H21D···O11	0.850	2.059	2.906	174.25	-x+1, -y+1, -z+1
O22-H22C···N7	0.850	1.969	2.817	175.48	
O22-H22D···O18	0.851	2.136	2.981	172.16	-x+1, y-1/2, -z+3/2
O23-H23C···O20	0.851	1.994	2.839	171.75	x, y-1, z
O23-H23D···O22	0.851	2.110	2.955	171.68	

5

N7-H7A···O8	0.860	1.994	2.846	170.66	-x+1, y+1/2, -z+1/2
N7-H7B···O16	0.860	2.102	2.950	168.36	-x+2, y+1/2, -z+1/2
N8-H8A···O7	0.860	2.002	2.859	174.10	-x+1, y-1/2, -z+1/2
N8-H8A···O14	0.860	2.319	3.132	157.79	-x+2, y-1/2, -z+1/2
O1-H1C···O22	0.850	1.979	2.672	137.99	
O1-H1D···O24	0.850	2.619	3.316	140.14	-x+3/2, -y+1, z-1/2
O2-H2C···O22	0.850	1.767	2.612	172.72	-x+2, y-1/2, -z+1/2
O2-H2D···O24	0.850	1.852	2.699	174.07	-x+3/2, -y+1, z-1/2
O9-H9A··O14	0.820	1.844	2.648	166.26	x-1/2, -y+3/2, -z
O10-H10···O21	0.820	2.229	2.946	146.08	x-1/2, -y+3/2, -z
O11-H11A···O16	0.820	1.817	2.623	167.33	x-1/2, -y+1/2, -z
O12-H12A···O17	0.820	1.932	2.721	161.22	x+1/2, -y+3/2, -z
O14-H14C···O17	0.850	1.871	2.721	179.24	x+1, y, z
O17-H17C···O5	0.850	2.404	3.244	169.47	x-1/2, -y+3/2, -z
O17-H17B···O24	0.865	2.048	2.912	176.91	x-1/2, -y+3/2, -z+1
O18-H18E···O7	0.850	2.218	3.034	160.80	x-1/2, -y+3/2, -z+1
O18-H18F···O10	0.850	2.354	3.168	160.41	x-1/2, -y+3/2, -z+1
O19-H19D···O10	0.850	2,327	3.159	166.17	x, y-1, z+1
O19-H19BD···N7	0.850	2.417	3.100	137.81	-x+3/2, -y+1, z+1/2
O21-H21E···O4	0.979	1.567	2.542	173.58	
O24-H24C···O11	0.850	1.844	2.693	178.02	x, y, z+1
O24-H24D···O19	0.850	1.904	2.754	177.62	x-1/2, -y+1/2, -z+2

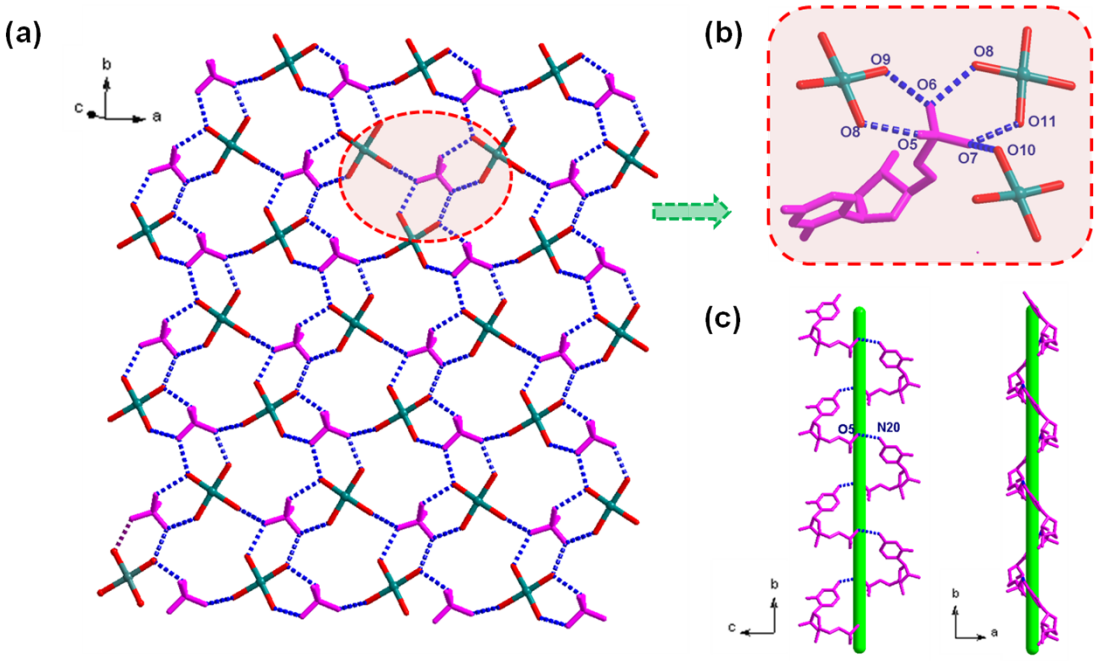

Figure S8. (a) 2D Hydrogen bonding layer of complex **1** in *ab* plane formed by hydrogen bonds between coordination water molecules and accepter atoms of CMP^{2-} ligands. (b) Perspective view of hydrogen bonds between CMP^{2-} ligands and coordination molecules. (c) Supramolecular helix formed by CMP ligands in the form of head-to-tail through hydrogen bonding (N20-H20B ··· O5, 2.849Å and 168.75 °).

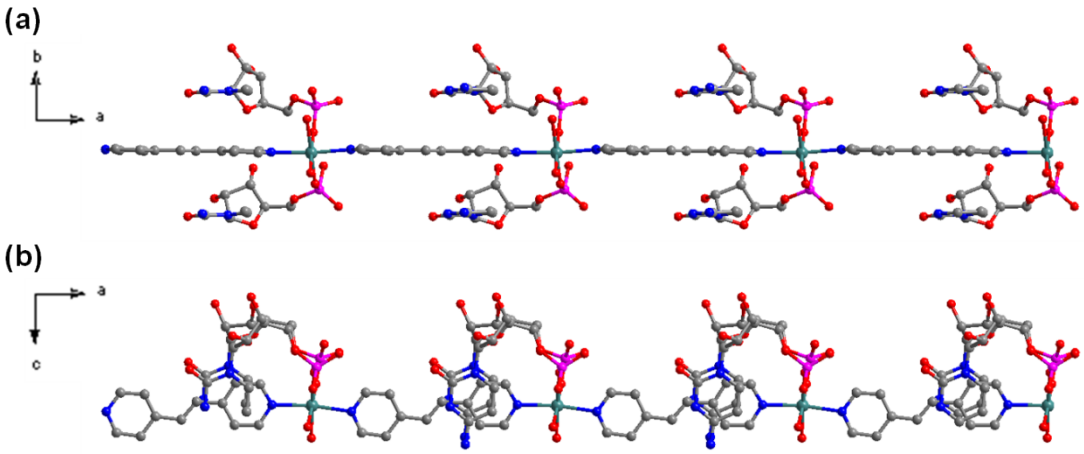

Figure S9. 1D chain of **2** viewed down from *c* axis (a) and *b* axis (b).

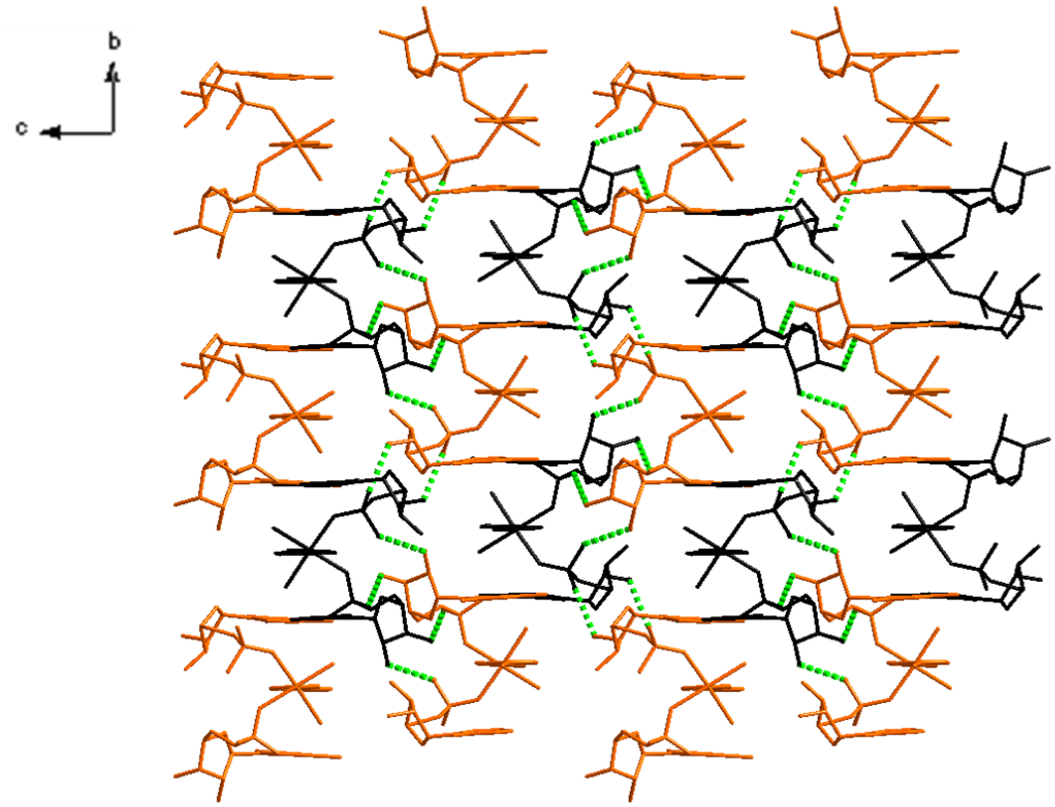

Figure S10. The 3D stacking structure picture of **2** assembled from interlayer hydrogen-bonding interactions viewed down from *c* axis.

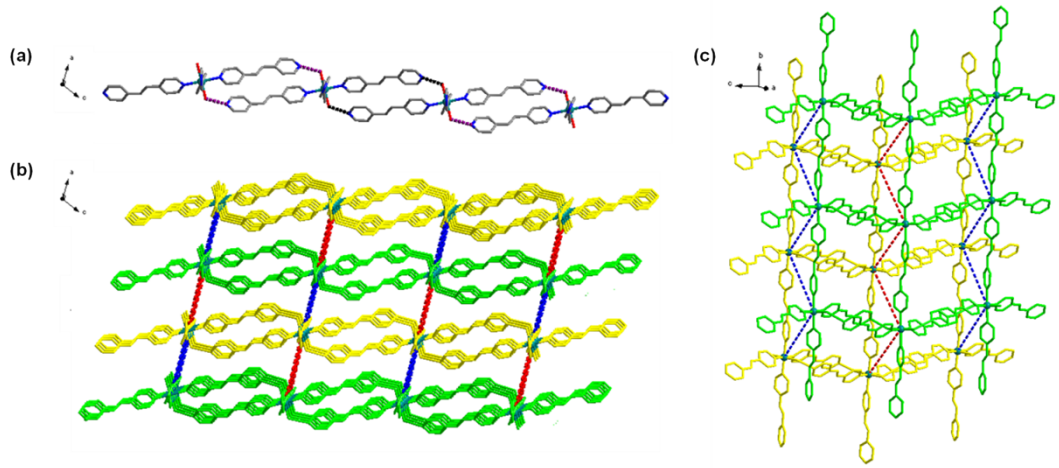

Figure S11. (a) 2D layer of **3** formed by inter-linear hydrogen bonding. (b)Two kinds of Mn⋯Mn distance between layers shown in red and blue dotted lines, respectively. (c) Two adjacent layers with 2D grid structure in **3**.

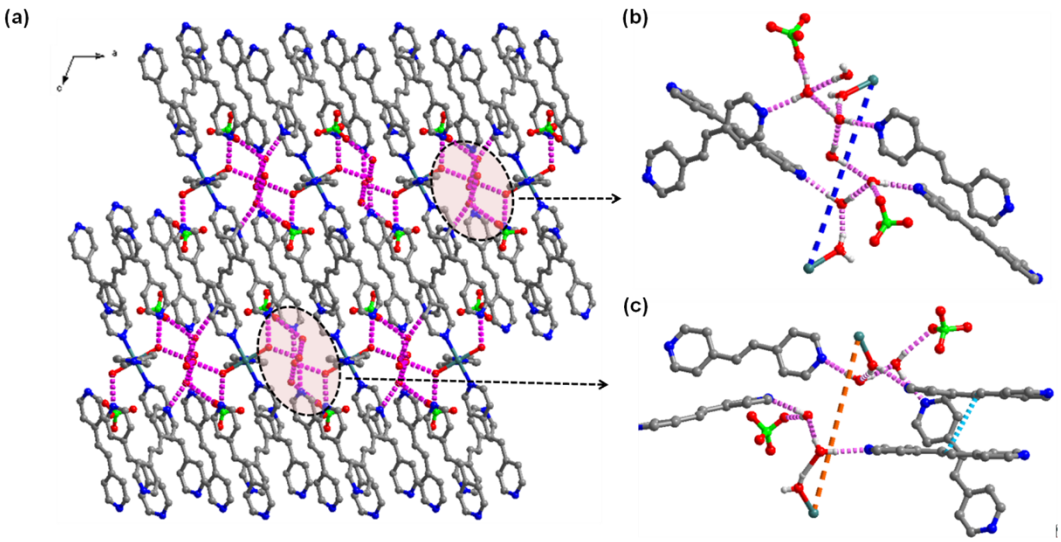

Figure S12. 3D supramolecular architecture of **3** assembled by noncovalent interactions (b and c), including hydrogen bonds formed between coordinated water molecules and free bpe, ClO_4^- or water molecules, as well as π-π stacking between adjacent bpe molecules.

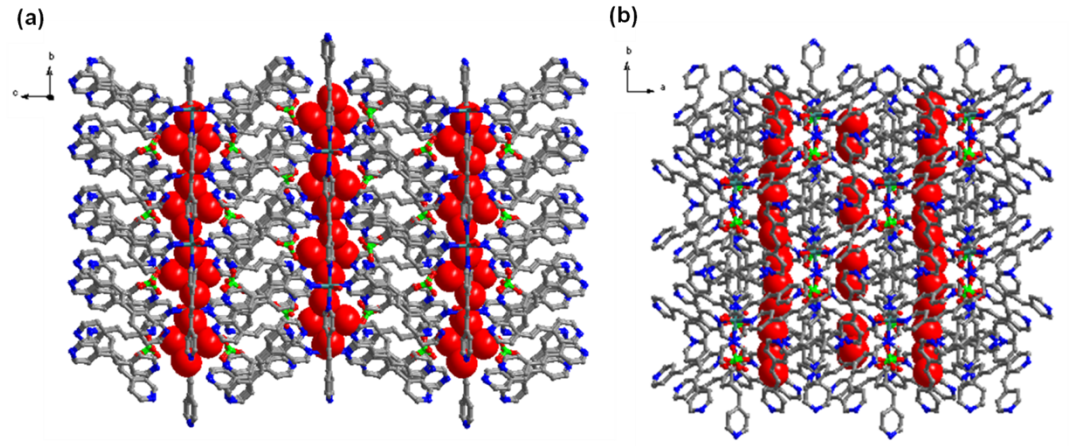

Figure S13. 3D supramolecular architecture of **3** with 1D channels filled with guest water molecules((a) viewed down from *a* axis, and (b) from *c* axis).

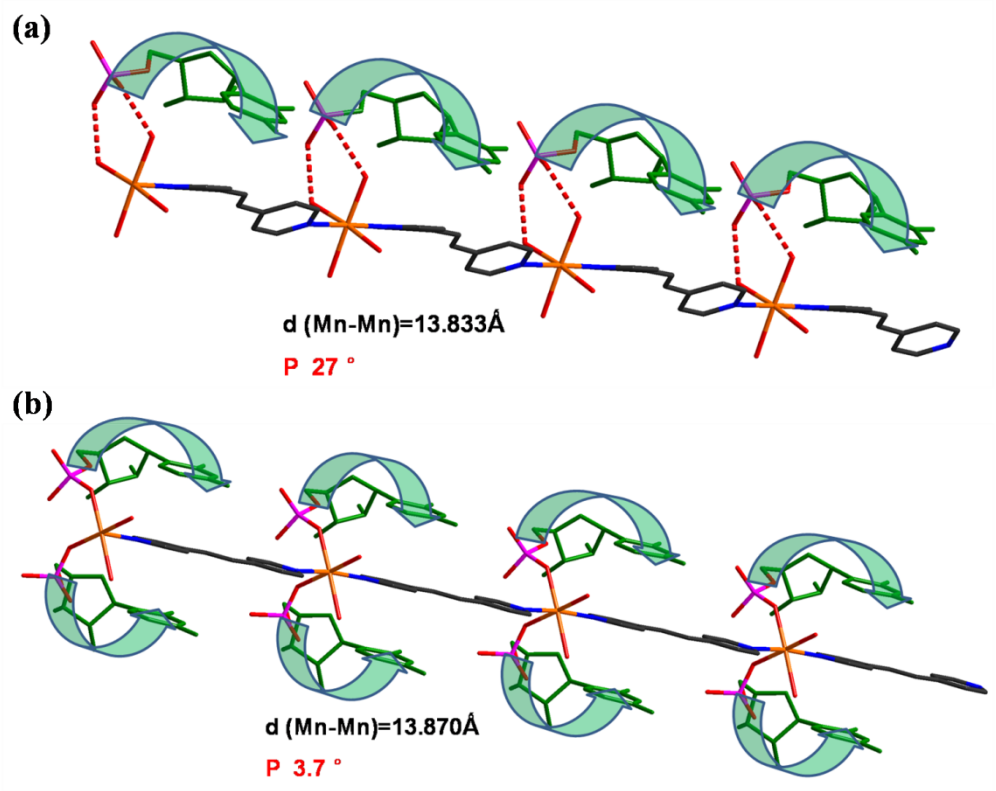

Figure S14. (a) P-EAC in **1** with clockwise orientated CMP ligand surrounding the axis of bpe. (b) P-EAC in **2** with equal clockwise and counterclockwise orientated chiral inducers surrounding the axis of bpe.

Section 3 XRPD Patterns and IR spectra

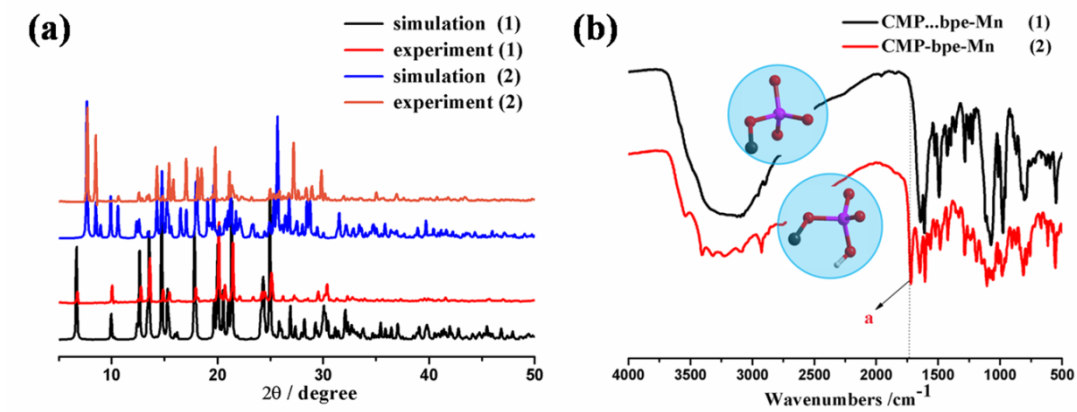

Figure S15. (a) PXRD patterns show the comparison between the experimental value and simulated ones for complexes **1** and **2**. **1** and **2** prepared under different acidic conditions show different structures. (b) IR spectra of complexes **1** and **2**. A new absorption *a* appeared in the spectrum of **2** because there is one more P-O Vibration mode, which can be explain by the protonation of one phosphate oxygen atom at more acidic condition.

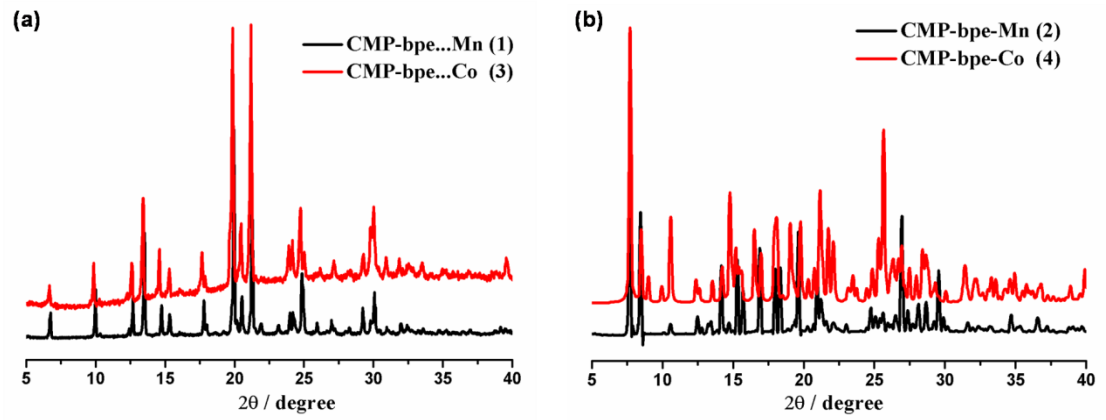

Figure S16. Comparison of PXRD patterns between **1** and **3** (a) as well as **2** and **4** (b). It is clearly that complexes of different kinds of metal ions adopt the same structure at similar acidity conditions.

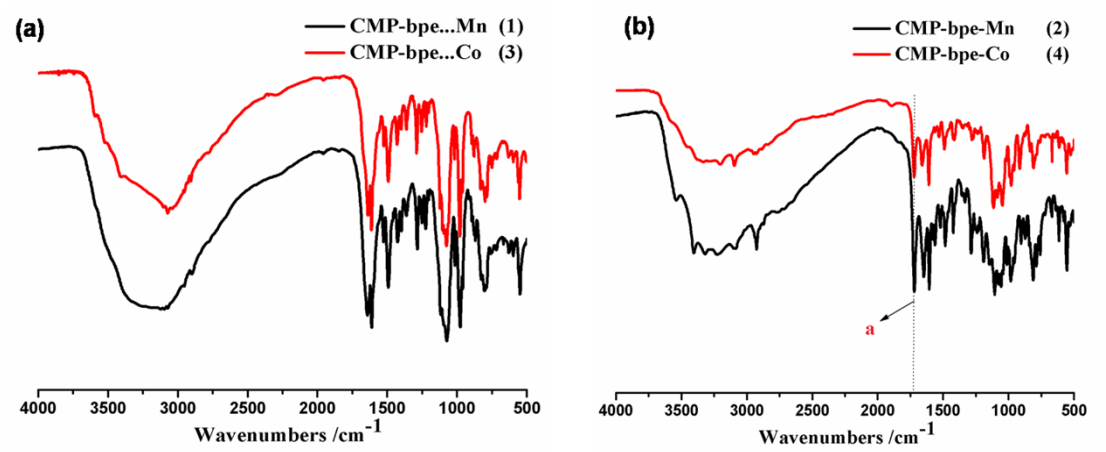

Figure S17. IR spectra of complexes **1** and **3**(a) as well as **2** and **4** (b). A new absorption peak ***a*** appeared in the spectra of **2** and **4** because there is one more P-O Vibration mode, which can be explain by the protonation of one phosphate oxygen atom at more acidic condition.

Section 5 Liquid-State CD Spectra.

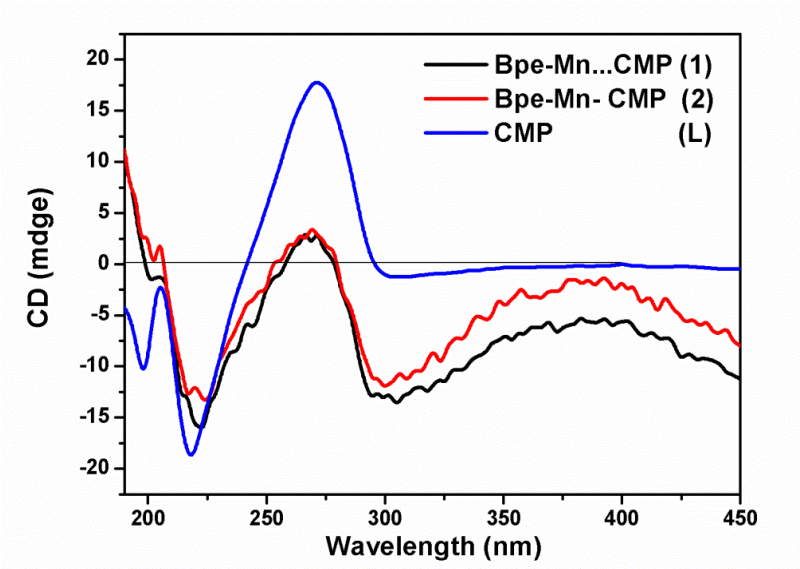

Figure S18. The liquid-state CD spectra of CMP ligands and its complexes **1** and **2** in water at 20℃. The spectra was obtained by measuring a 0.02mM solution in a 1mm cell. The typical CD spectrum of CMP illustrates that the nucleotides ligand is D-ribonucleotide, which has a positive band near 271nm. The weak negative band centred at 300nm in the spectra of **1** and **2** demonstrates there exist interaction between CMP ligand and the metal ions, which can prevent the mutarotation, making ligands keep the β-anomers in their complexes.

Section 6 Solid-State UV-vis Spectra.

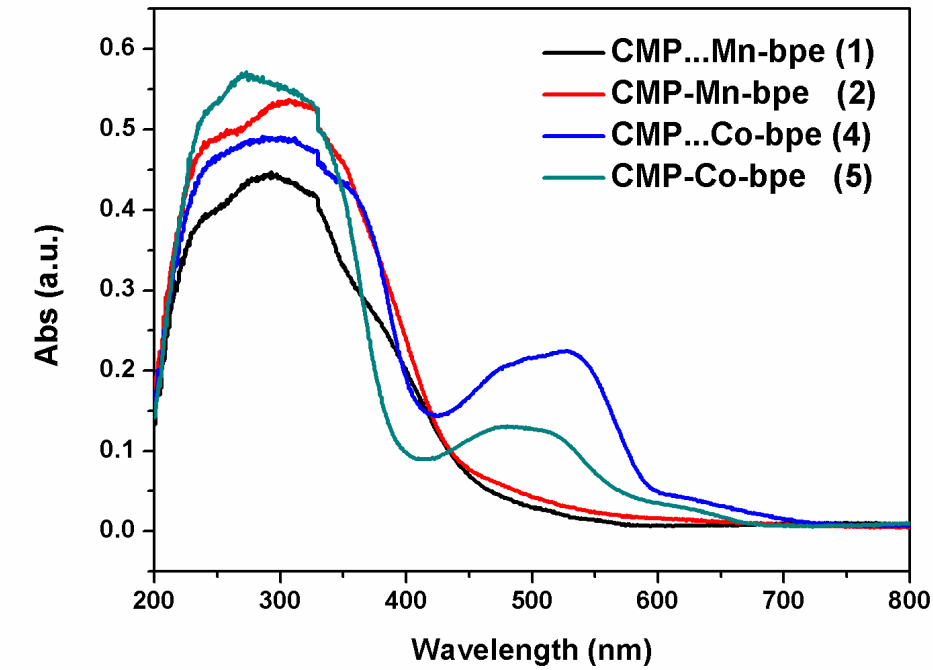

Figure S19. The solid-state UV-vis spectra of complexes **1**, **2**, **4**, **and 5** at room temperature. There exist d–d electron transitions in the region of 400-600nm for complexes **4** and **5**.

Section 7 TGA (Thermogravimetric Analysis).

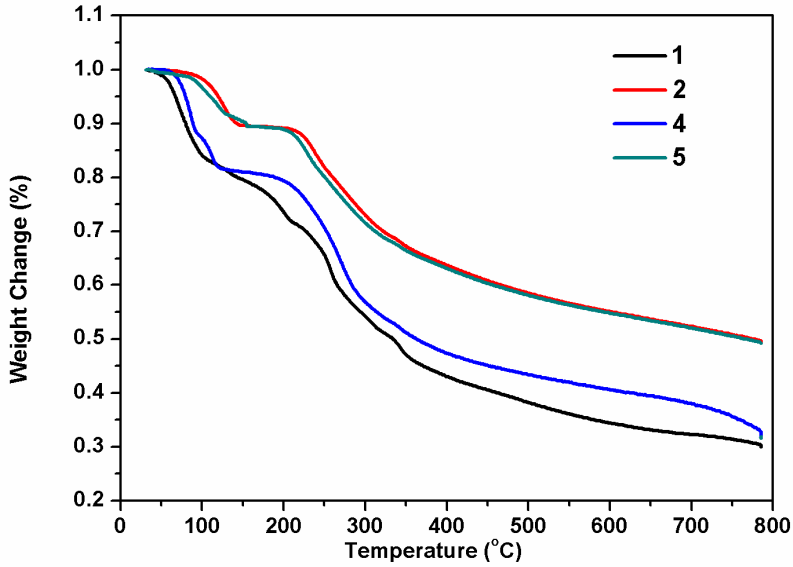

Figure S20. TG analysis curves of **1**, **2**, **4**, and **5**. The mass loss of ca. 18.41 % from 80.2 °C to 122.4 °C is related to the loss of guest water solvates and coordinated water molecules (calculated value 18.32 %) for **1**. And it begin to collapse at about 200.0°C. The first weight loss stage of **2** is from 99.8°C to 144.9 °C, and the mess loss (cal.10.09%, calculated value 10.22%) is also related to the loss of guest and coordinated water molecules. Complex **2** showed better thermal stability than **1**, the collapse temperature of which is about 221.5°C. The thermal properties of **4** and **5** are similar to **1** and **2**, respectively, which give reasons that there are three guest water molecules in complex **4**. However, the TG analysis of **3** is not studied because of its explosive components (ClO_4^-).

Section 8 Crystal-to-crystal transformation.

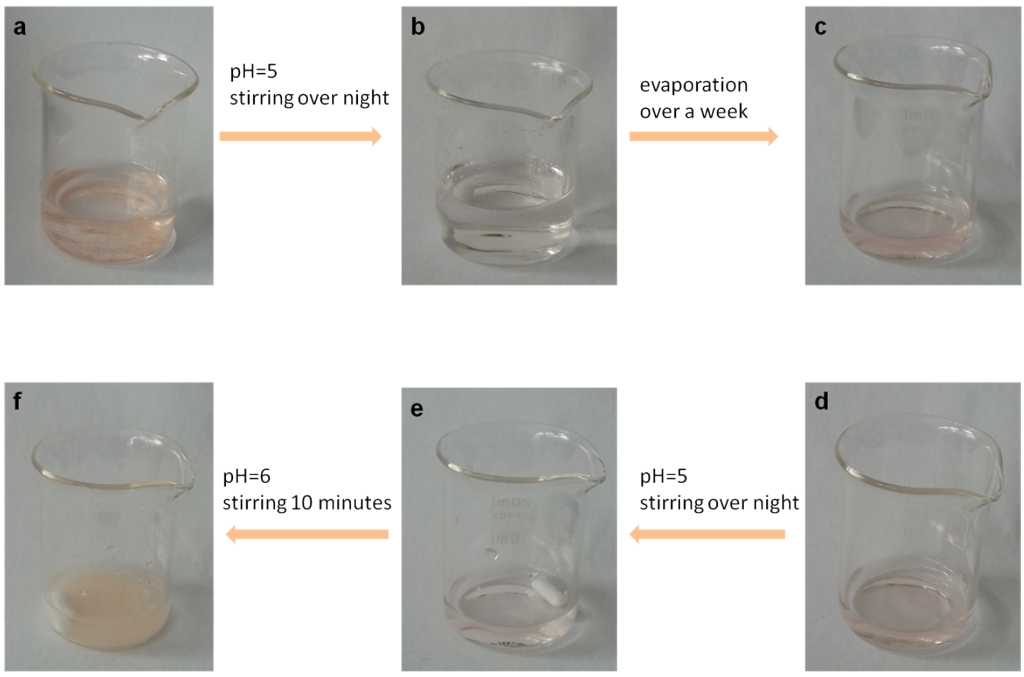

Figure S21. Crystal-to-crystal transformation from **4** to **5** (*a* to *c*), and from **5** to **4** (*d* to *f*).

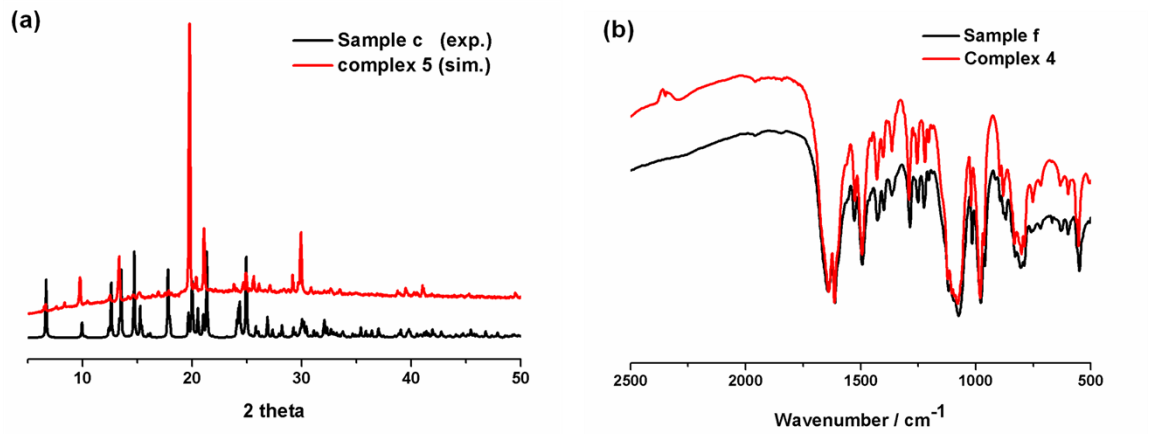

Figure S22. (a) Comparison between crystal transition product ***c*** (crystalline) and complex **5** by the methods of PXRD. (b) Comparison between crystal transition product ***f*** (powder) and complex **4** by the methods of IR.